Available online at www.sciencedirect.com
ScienceDirect
Applied Catalysis B: Environmental 80 (2008) 81–87
APPLIED CATALYSIS B: ENVIRONMENTAL
www.elsevier.com/locate/apcatb

Preparation of a visible sensitive carbon doped TiO_2 photo-catalyst by grinding TiO_2 with ethanol and heating treatment

In-Cheol Kang *, Qiwu Zhang, Shu Yin, Tsugio Sato, Fumio Saito

Institute of Multidisciplinary Research for Advanced Materials, Tohoku University, Sendai 980-8577, Japan

Received 29 June 2007; received in revised form 2 November 2007; accepted 3 November 2007
Available online 19 November 2007

Abstract

We have synthesized a carbon doped titanium oxide powder (C-TiO_2) which is a photo-catalytic material acting under irradiation of light of wave length in visible region, by mechanochemical (MC) and heating operations. The MC operation is conducted by grinding TiO_2 with ethanol (C_2H_5OH) in air, and the heating is carried out at different temperatures in air. The prepared samples were characterized by a series of analytical methods including X-ray diffraction, thermogravimetry-mass spectroscopy, Fourier transform infrared spectroscopy, specific surface area measurement, X-ray photoelectron spectroscopy (XPS), NO_x gas decomposition and ultraviolet visible spectroscopy (UV–vis). XPS analysis particularly demonstrates the existence of C–Ti and C–O bindings, to which the improvement in photo-catalyst is attributed.

Keywords: Grinding; Carbon doping; Carbonate species; Solid–liquid reaction; TiO_2 photo-catalyst

1. Introduction

A titanium di-oxide (TiO_2) has been considered as a promising photo-catalytic material for water and air purification [1–3], water splitting [4,5], conversion of solar energy to electrical and chemical energy [6] due to its good chemical and photonic stability, and relatively good reactivity [1,7,8]. However its wide band gap of 3.2 eV has limited the activity under ultraviolet irradiation region. In order to utilize wider range of solar energy, lots of efforts have been made to narrow band gap by doping non-metal elements such as nitrogen [9–12], carbon [13–22] and sulfur [23–25]. As a result, visible-light sensitive photo-catalytic materials could be achieved by narrowing band gap via overlapping between O_{2p} orbital and $C_{2p}/N_{2p}/S_{3p}$ orbital. On the other hand, transition metal doping [26–28] has been also effective to develop high photo-catalytic activity by decelerating recombination rate between photo-excited electrons and holes.

In particular, with respect to a carbon (C) doped TiO_2 photo-catalyst, based on the theoretical calculation of electronic density of states (DOS), Asahi et al. [10] have proposed that the C_{2p} states were too deep in the band gap of TiO_2 and it is difficult to overlapped C_{2p} states over O_{2p} states. However, Wang and Lewis [14] have proposed that the significant overlap between C_{2p} states and O_{2p} states is possible when more carbon impurities substitute for oxygen atoms (about 5.2%). Accordingly, a C doped TiO_2 has been well known as a sensitive photo-catalyst under visible irradiation region. Besides, according to the result of Janus et al. [13], photo-catalytic ability of C doped TiO_2 could be improved by decreasing the recombination rate in photo-generated electron–hole pair by the existence of electron scavenger carbon doped into TiO_2. The nature of the carbon-induced modifications of the TiO_2 electronic band structure remained unclear, and the enhancement of photo-catalytic activity was attributed to either the band gap narrowing [14–17] or the formation of localized mid-gap state [17–19] in TiO_2 band gap. One possible reason may lie at the special existing states of carbon. It may combine with oxygen by substituting titanium as the transition metal doping or with titanium by substituting oxygen as the non-metal element doping. This has been addressed by several investigations where XPS analysis particularly has been used to reveal the two binding energy positions with C doped TiO_2 at 282 eV [15] and 288.6 eV [19,20]. The observed phenomena vary depending on the preparing conditions.

* Corresponding author. Tel.: +81 22 217 5136; fax: +81 22 217 5136.
E-mail address: kic22@andy.tagen.tohoku.ac.jp (I.-C. Kang).

0926-3373/$ – see front matter © 2007 Elsevier B.V. All rights reserved.
doi:10.1016/j.apcatb.2007.11.005

On the other hand, regarding the synthesis methods for carbon doping, the processes used are quite complicated and needing elaborate controlling. The agents used are not easily available and needing careful handling. There needs further improvement by novel development. This work is performed based on two purposes; one is to develop a simple process to allow the use of easily available commercial chemicals as starting materials. The process consists of mechanochemical treatment, followed by heating. Another is to study the existing state of carbon in the product and the effect on its photocatalytic activity when irradiation of light having the range of visible wave length of light.

2. Experimental

2.1. Samples, grinding and heating operations

Anatase titania powder (TiO_2) and ethanol were supplied from Wako Pure Chem. Inc., Japan and used as starting materials. A planetary ball mill (Pulverisette-7, Fritsch, Germany) was used to grind the sample. The mill consists of a set of pot made of partial stabilized zirconia (PSZ) having 45 cm^3 in inner volume, in which seven zirconia balls of 15 mm in diameter and starting material TiO_2 and ethanol at 5% in mass were put. Total 4 g of TiO_2 powder and ethanol were put into the pot, and then the grinding was operated at 700 rpm for various grinding periods of time ranged from 15 to 240 min. The ground samples were subsequently heated at the rate of 200 °C/h up to 200 °C for 60 min in air to remove impurities from the ground products. The heating up to 400 °C was attempted as a reference.

2.2. Characterizations

The crystallinity of the ground and heated products were analyzed by XRD (RAD-B, Rigaku Co. Ltd., Japan) using Cu Kα radiation. The crystallite size (D) was calculated by following Scherrer's formula depending on the period of grinding operation time:

$$D = \frac{0.9\lambda}{\beta_{1/2}\cos\theta}$$

where λ is the wavelength (0.15418 nm) of the X-ray, $\beta_{1/2}$ is line-width at medium height of anatase peak (1 0 1) and rutile peak (1 1 0), and θ is the diffracting angle [29].

The average crystallite was calculated by following equation:

$$D_{ave} = D_a\left(\frac{I_a}{I_a + I_r}\right) + D_r\left(\frac{I_r}{I_a + I_r}\right)$$

where D_{ave} is average crystallite size, D_a and D_r are crystallite size of anatase peak (1 0 1) and rutile peak (1 1 0), respectively. I_a and I_r are peak intensity of anatase (1 0 1) and rutile (1 1 0), respectively.

The specific surface area (SSA) of the products was measured by nitrogen adsorption–desorption isothermal measurements at 77 K (ASAP-2010, Micromeritics, Shimadzu Co. Ltd., Japan) based on BET method. The optical absorption edge of the products under irradiation of light was measured by an UV–vis spectrophotometer (UV-2000, Shimadzu, Japan) from 700 to 200 nm in wavelength region. Infrared spectra were recorded with 4 cm^{-1} resolution by an FT-IR spectrometer (FTS 7000, Mid & ATR) ranged from 1000 to 3000 cm^{-1} in wavelength. Thermogravimeter mass spectrometer (TG-MS) (Thermo Plus TG 8120, Rigaku Co. Ltd., Japan) was operated in He atmosphere of 300 ml/min flowing rate with increasing rate of 20 °C/min to 800 °C for understanding the decomposition behavior of the products. X-ray photoelectron spectroscopy (XPS) (PHI 5600 ESCA system, Ulvac-Phi. Inc., Japan) was conducted to have the information on chemical binding energy of the products. After the products were sputtered with 3 kV Ar^+ ion for 5 min, on 4 mm × 4 mm area, the XPS scanning was recorded with Mg Kα X-ray by 20 times × 3cycles.

NO_x gas decomposition was measured for examining photocatalytic activity of the products. The NO_x gas at the outlet of reactor box (373 cm^3) was flowed in and the concentration of NO_x gas was measured at the outlet with 1 ppm NO_x–50 vol.% air mixed gas at flowing rate of 200 cm^3/min. The decomposition test was carried out as following: the photo-catalyst product was put on a hollow place of 20 mm × 15 mm × 0.5 mm on a glass holder plate and set in the center of the reactor. A 450-W high-pressure mercury lamp (the irradiation intensity was set in 1000 (μmol/s m^2)/μA by lighter meter (Model; LI-189, Serial NO; LM 1322)) was used as the light source, in which the wavelength was controlled by various filters, i.e., Pyrex glass for cutting off the light of wavelength <290 nm, Kenko L41 Super Pro (W) filter <400 nm and Fuji, tri-acetyl cellulose filter <510 nm [30].

3. Results

3.1. Effect of grinding periods of time

Fig. 1 illustrates XRD patterns of the samples ground with ethanol for different periods of time. The profiles of (a–g) are of raw-TiO_2, products ground for 15 min, 30 min, 60 min, 120 min, 180 min and 240 min, respectively. A, R, S and Z represent anatase, rutile, srilankite phases of TiO_2 and ZrO_2 which came from wear of balls and pot of the mill caused by the grinding operation with ethanol. With increasing in grinding time, the anatase phase was changed into srilankite (high pressure phase), and from srilankite to rutile phase (stable phase). After 240 min grinding operation, almost all anatase phase was changed into rutile one. This demonstrates that mechanical energy makes anatase transfer to rutile (high temperature stable phase) at room temperature. After 60 min grinding operation, new peak positioned at 30° is attributed to ZrO_2 impurity. The peak intensity of ZrO_2 looks to be higher than that of the products ground in NH_3 gas ambient, according to our data [9] even at the same operating time. In other words, solid/liquid grinding accelerates wear from the grinding media rather than that of the case of solid/gas co-grinding operation.

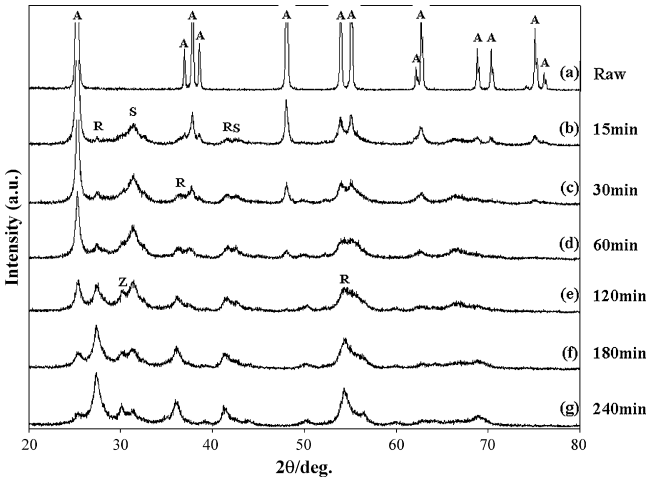

Fig. 1. XRD patterns of the samples ground with ethanol for different periods of time. (a) Raw-TiO_2, (b) ground for 15 min, (c) 30 min, (d) 60 min, (e) 120 min, (f) 180 min and (g) 240 min, respectively (A: anatase, R: rutile, S: srilankite, Z: zirconia).

Furthermore, the wear rate of grinding medium (ZrO_2 pot and ball) increased with increasing in the added ethanol amount, whereas the phase transformation rate from anatase to rutile decreased.

Fig. 2 shows specific surface area (SSA) (S) and crystallite size (G) of the products ground for different periods of time. With the SSA value of raw-TiO_2 of 10 m^2/g, the SSA value of products gradually increases with an increase in grinding time and reaches over 50 m^2/g at 120 min grinding, while no further change is observed over 120 min. The reason why the products exhibit such high SSA value and no decrease in SSA is observed with prolonged grinding, which has been usually observed due to agglomeration, may be attributed to the existence of impurity on the surfaces of the sample during grinding operation. The impurity composition on the surfaces, which is finally removed by heating operation, may prevent the agglomeration of particles and further information will be described in FI-IR analysis. The comparison between the product ground for 120 min with ethanol (5 wt%) and the product ground for 120 min without ethanol (a) clearly confirm it, where large difference in SSA of two samples is observed. And with crystallite size of products, the crystallite size decreased gradually with an increase in grinding time and reached below 15 nm in diameter at 120 min grinding time. This result verifies that the ethanol addition results in enhancing photo-catalytic activity via carbon doping and prevention of particle agglomeration. Although it has been known that the change of phase structure has influence on the photo-catalytic activity; e.g. synergetic effect via mixture of anatase and rutile TiO_2 [31], it has been reported that both doped and undoped products ground for 120 min have clearly different photo-catalytic activity even with similar phase structures [24]. Namely, the effect of doping and prevention of particle agglomeration rather than phase structure on photo-catalytic activity are dominant.

Fig. 3 shows UV–vis patterns of products with grinding periods of time. This indicates an irradiation-absorbing edge, and compared with that of the raw TiO_2 sample, not only the optical absorption edge of products has been shifted to the lower-energy region but also the absorbance is sensitive with progress of grinding. This suggests that the sample has been modified with impurity doping due to the grinding operation.

Fig. 4 illustrates photo-catalytic activity represented by the decomposition rate of NO_x gas as a function of grinding time from (a) raw-TiO_2 (0 min) to (g) 240 min. In the irradiation of visible light region, the NO_x gas degradation rate gradually increases with an increase in grinding periods of time. Finally, the (e) product ground for 120 min demonstrates the highest NO_x gas decomposition activity under visible light irradiation. One reason for the improvement in photo-catalytic activity is the increase of specific surface area shown in Fig. 2. However, the prolonged grinding operation over 120 min induces slight reduction in NO_x gas decomposition activity in visible light region even at similar specific surface area compared to a (e) product ground for 120 min.

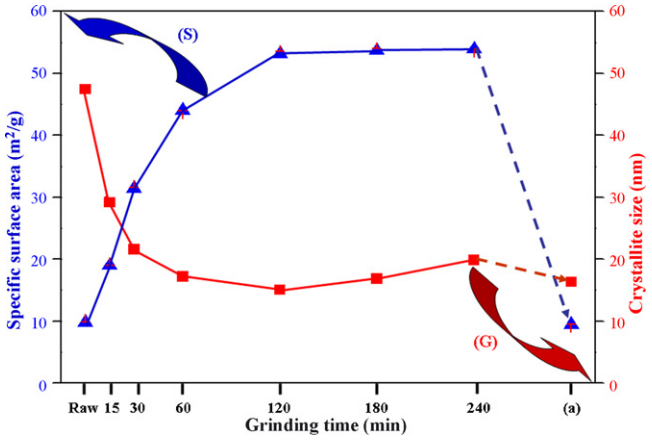

Fig. 2. Specific surface area (S) and average grain size (G) of the products ground with ethanol for different periods of time. (a) is results of product ground for 120min without ethanol addition (all results are of products heated at 200 °C).

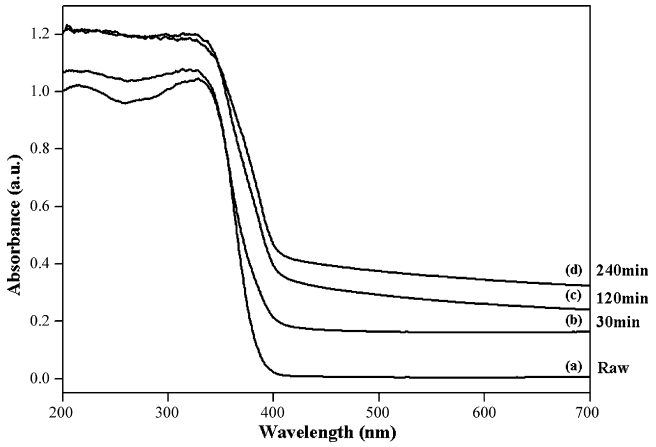

Fig. 3. UV–vis patterns of the products ground with ethanol for different periods of time. (a) Raw-TiO_2, (b) ground for 30 min, (c) 120 min and (d) 240 min.

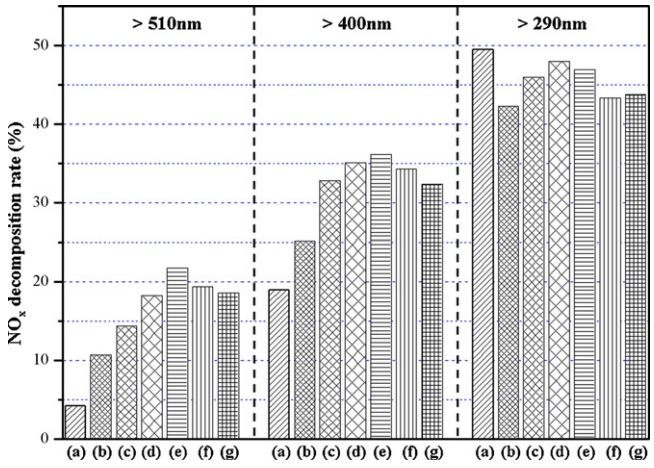

Fig. 4. NO gas decomposition activity of the products ground with ethanol for different periods of time. (a) Raw-TiO_2, (b) a product ground for 15 min, (c) a product ground for 30 min, (d) a product ground for 60 min, (e) a product ground for 120 min, (f) a product ground for 180 min and (g) a product ground for 240 min.

3.2. Effect of heating temperature

The post-heating operation is one of important procedures on formation of high utility photo-catalyst because thermal treatment affects crystallinity, specific surface area, surface purity and existence of surface hydroxyl group.

Fig. 5 displays XRD patterns of (a) raw-TiO_2, (b) a green product (without heating treatment), (c) a product heated at 200 °C and (d) a product heated at 400 °C, respectively. As a result of comparison of crystallinity between (b), (c) and (d), it can be recognized that the crystallinity was enhanced with increase in heating temperature. In general, although photo-catalytic activity is proportional to crystallinity it is always not right with the doped sample, because the high temperature heating operation may induce the decrease in specific surface area, the removal of surface hydroxyl group and make the doped carbon be withdrawn from TiO_2 lattice. The (b) product, TiO_2 ground with ethanol for 2 h, was heated at 200 °C (c) and 400 °C (d) for 1 h in air, respectively.

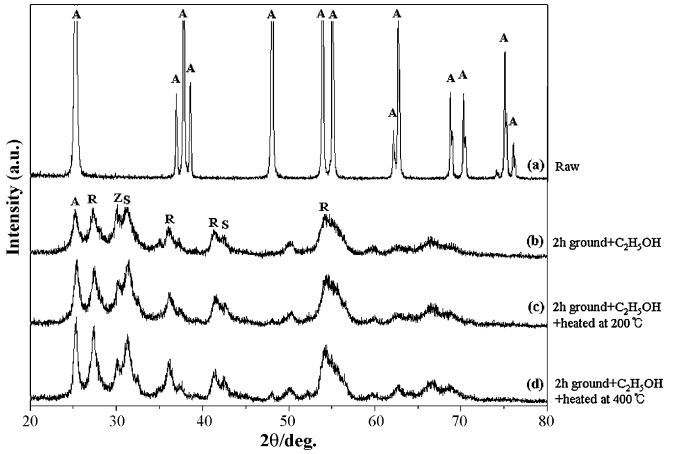

Fig. 5. XRD patterns of raw-TiO_2 and products ground for 2 h and heated at 200 and 400 °C (A: anatase, R: rutile, Z: zirconia, S: srilankite).

Fig. 6 shows specific surface area (SSA) of products, (a–d); (a) is the raw-TiO_2, (b) the green product (without heating), (c) the product heated at 200 °C, (d) the product heated at 400 °C. The (c) product heated at 200 °C shows a higher specific surface area than that of green product (b), which may be due to the elimination of the surface impurities adsorbed on TiO_2 surface by heating operation. More evidence will be shown in Figs. 8 and 9. On the contrary, the (d) product heated at 400 °C shows a low specific surface area compared with the (c) product heated at 200 °C even and (b) green product. It seems that particle size has grown up due to high treatment temperature. This result suggests that the suitable operating temperature must be considered. The (e) is the raw-TiO_2 ground for 2 h and heated at 200 °C for 1 h in air, which is a reference for explaining influence of ethanol addition on SSA value. The comparison between (c) and (e) products explains that the ethanol addition in the grinding operation improves specific surface area due to the decrease of particle size via prevention of particle agglomeration during grinding and carbon doping.

Fig. 7 illustrates NO_x gas decomposition activity as a post-heating operating temperature. In the order (a–d) are of raw-TiO_2, green product, a product heated at 200 °C and a product heated at 400 °C in air. The comparison of (b) and (c) products shown in Fig. 7 illustrates the importance of post-heating treatment, i.e., importance of surface purity. Namely, (c) the heated product shows a higher NO_x gas decomposition activity than that of (b) green product under irradiation of light in whole wavelength region. In comparison of both products (b) and (d), even though the specific surface area of the product (b) (green product) is larger than that of the product (d) heated at 400 °C, NO_x gas decomposition activity of the green product (b) in visible light irradiation is weaker than the others. This result emphasizes again an importance of surface purity, because surface impurity prevents optical irradiation to surface of TiO_2 for redox reaction.

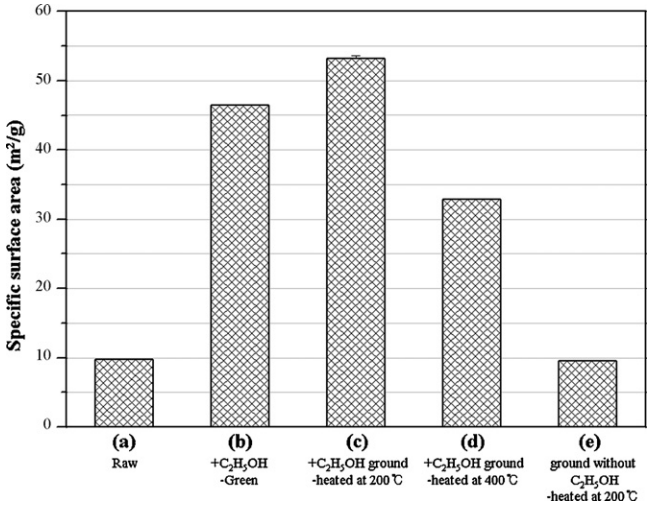

Fig. 6. Specific surface area of products; (a) raw-TiO_2, (b) a product without heating (green product), (c) a product heated at 200 °C and (d) a product heated at 400 °C for 1 h in air; (e) raw-TiO_2 ground without addition of ethanol for 2 h followed by heating at 200 °C for 1 h in air.

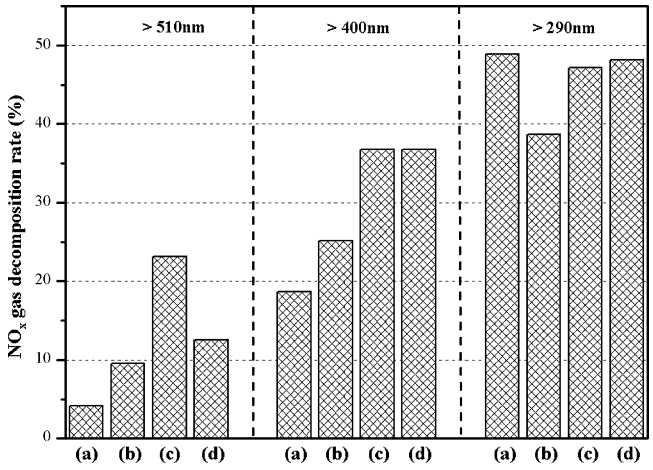

Fig. 7. NO_x gas decomposition activity with post-heating operation conditions; (a) raw-TiO_2, (b) a product without heating (green product), (c) a product heated at 200 °C and (d) a product heated at 400 °C for 1 h in air.

The result for both products (c) and (d) is difficult to understand the difference in SSA shown in Fig. 6. The NO_x gas decomposition activity of the product (d) is lower than that of the product (c) over 510 nm in wavelength region, while the activity of the products (c) and (d) is similar below 510 nm in wavelength region. The smaller SSA value of the sample (d) does not explain the similar NO_x gas decomposition activity of both samples under irradiation of the light below 510 nm in wavelength and ultra violet region. This will be discussed with the data obtained by XPS analysis shown in Fig. 10.

Our previous paper [9] suggested an importance of surface purity for progressive NO_x gas degradation activity against whole irradiation wavelength. FT-IR analysis data shown in Fig. 8 well illustrate the importance of surface chemical composition of products as a function of heating temperature. While the raw-TiO_2 just possesses H_2O and hydroxyl group (noted by ⑨ located at 1620–1630 cm^{-1}) on TiO_2 surface, the others products possess various compositions related to

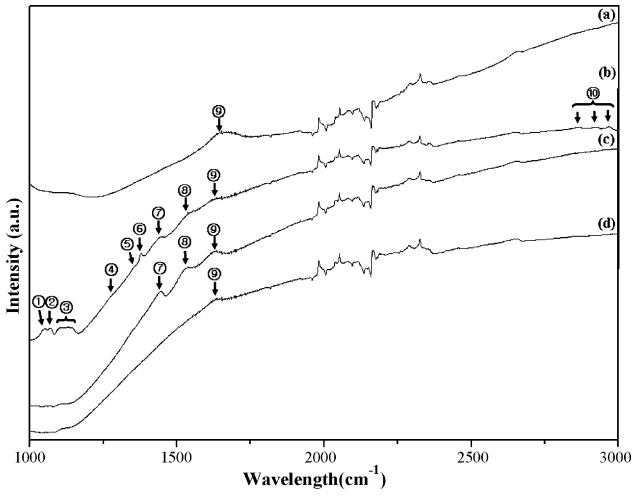

Fig. 8. FT-IR profiles of product ground for 2 h; (a) raw-TiO_2, (b) a product without heating (green product), (c) a product heated at 200 °C and (d) a product heated at 400 °C for 1 h in air.

ethanol. The peaks in spectrum of the sample (b) can be roughly ascribed to four kinds of compounds: ethoxide (①–③, ⑤), ethanol (④, ⑥, ⑩), acetate (⑦, ⑧) and water (⑨) [32,33]. The ethoxide was chemisorbed on TiO_2 surface via following reaction [33].

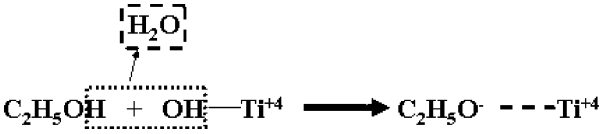

(1)

Reaction between H^+ of C_2H_5OH and OH^- adsorbed on Lewis acid Ti^{4+} induced formation of H_2O and bonding of $C_2H_5O^-$ (ethoxide) to Ti^{4+}. The ethanol was absorbed on the TiO_2 surface via following reaction [33]

(2)

The C_2H_5OH was strongly bonded to Lewis acid sites on Ti^{4+}, coordinatively. When comparing the spectrum of the sample (c) with that of the sample (b), it is clear that these ethoxide (①–③, ⑤) and ethanol (④, ⑥, ⑩) were eliminated by 200 °C post-heating operation with acetate complex (⑦, ⑧) and water (⑨) remaining on the sample. Furthermore, the 400 °C post-heating operation done in air eliminated even acetate complex from TiO_2 surface and resulted in decrease in hydroxyl peak intensity when examining the spectrum of sample (d).

Fig. 9 illustrates TG-MS profile of products with post-heating temperature, which helps to understand decomposition behavior of the products. The vertical value means a decomposed amount per product (1 mg). In (a)–(c), the observed H_2O composition is attributed to the absorbed moisture and hydroxyl groups on the prepared samples. The decomposed amount of H_2O and hydroxyl groups of (a) and (b) are similar, while that of (c) heated at 400 °C is decreased compared to that of (a) and (b) owing to removal of H_2O/hydroxyl groups by high heating operation (400 °C).

In the (a) product, decomposition of CO (marked by dot-spot) and CO_2 (marked by solid) started at around 300 °C and 400 °C, respectively. On the other hand, in the (b) product heated at 200 °C, the configuration with respect to decomposition of CO is not observed, whereas the decomposition of CO_2 is observed at around 400 °C. By comparing Fig. 8(b and c) with Fig. 9(a and b), it could be confirmed that the decomposition behavior around 300 °C is assigned to decomposition of ethanol and ethoxide adsorbed on TiO_2 surface, and the decomposition behavior about 400 °C is related to acetate complex adsorbed on TiO_2 surface. The sample (c) heated at 400 °C shows H_2O decomposition profile without elimination of CO/CO_2, which indicates that all of surface compositions were removed by heating at 400 °C. This result well agrees with that shown in Fig. 8. In the present study, heating operation performed in air ambient makes it possible to remove ethanol and ethoxide impurities from the product.

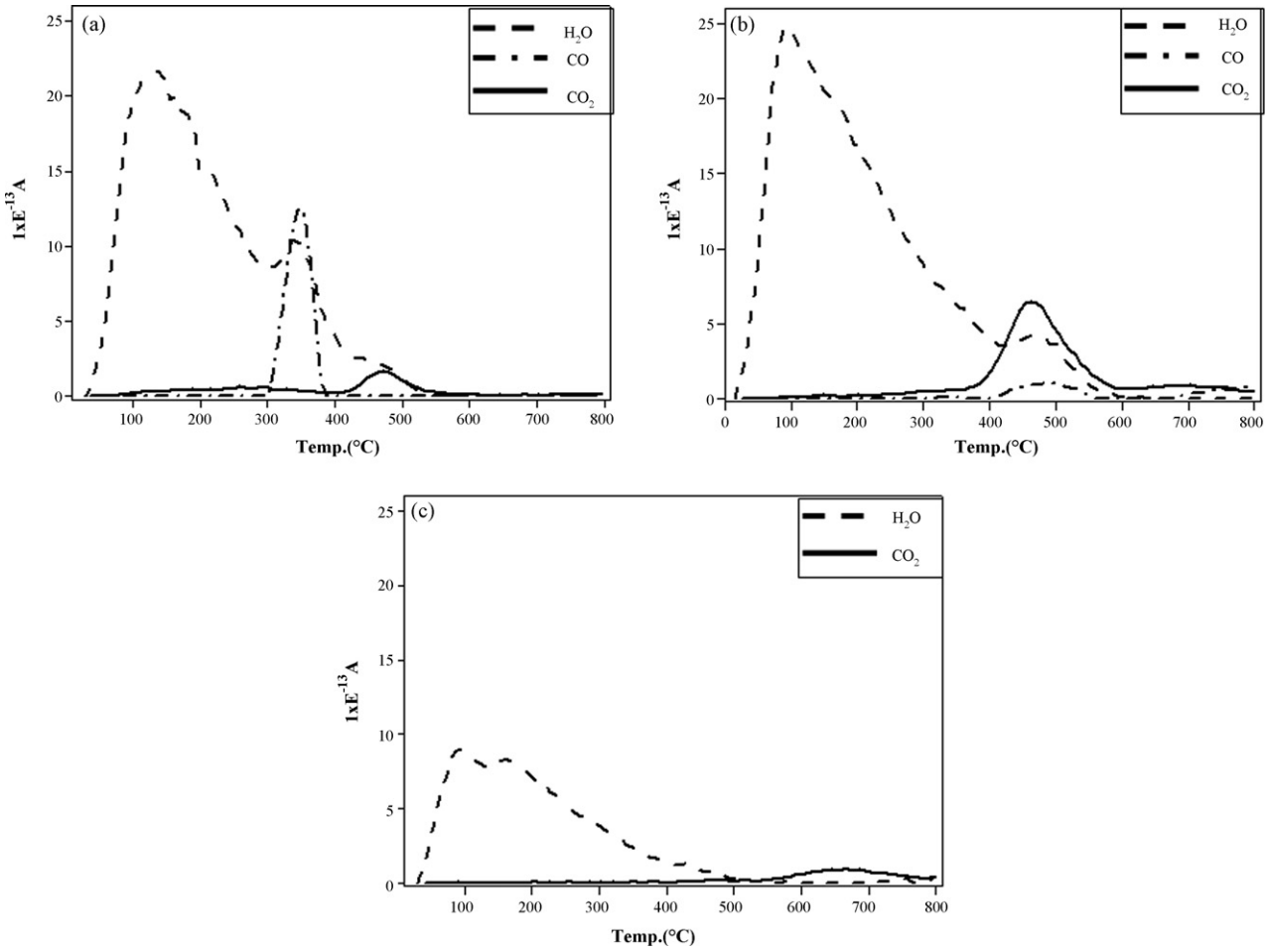

Fig. 9. TG-MS profiles of (a) green product, (b) a product heated at 200 °C and (c) a product heated at 400 °C for 1 h in air (TG-MS analyzes were measured in flowing He gas).

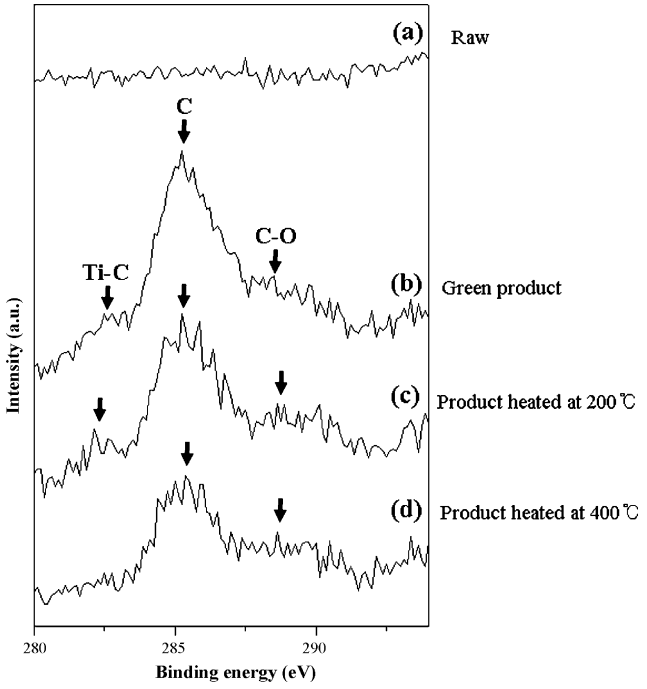

Fig. 10. XPS profiles of products; (a) a raw-TiO_2, (b) a product without heating (green product), (c) a product heated at 200 °C and (d) a product heated at 400 °C for 1 h in air.

Fig. 10 shows XPS profiles of the samples prepared. These profiles identify the chemical binding energy depending on the post-heat operating temperature. The (b) green product and a (c) product heated at 200 °C in air have Ti–C, C–O and C–C bindings. The binding energy at 282 eV is assigned to Ti–C bond [15] via substitution of carbon for oxygen site of TiO_2 during grinding operation. The C–O binding located at 288.6 eV is assigned to the existence of carbonate species [18,19,22] via substitution carbon for Ti site or interstitial of C into TiO_2 lattice during grinding operation. The C–C binding located at 285 eV is assigned to adventitious elemental carbon [19,20]. Anyhow, the product (d) heated at 400 °C displays C–C and C–O bindings without Ti–C binding, which means breakage of Ti-C binding by heating at 400 °C. This illustrates why the product heated at 400 °C shows lower NO_x gas decomposition activity than that of a product heated at 200 °C over 510 nm in wavelength irradiation as shown in Fig. 7, finally due to the breakage of Ti–C binding. Nevertheless, the existence of C–O binding (carbonate species) plays positive role on NO_x gas decomposition in irradiation of light having whole region in wavelength.

4. Discussion

In Fig. 7, the samples (b), (c) and (d) prepared at different heating temperatures showed different NO_x gas degradation

activity, particularly over 510 nm in wavelength region. The sample (c) heated at 200 °C showed higher photo-catalytic activity than that of (b) the green product and (d) the sample heated at 400 °C. The low photo-catalytic activity of (b) the sample might be ascribed to the existence of surface impurities such as ethanol and ethoxide, acetate complex, which was proven from the results shown in Figs. 8 and 9, namely the interference of these impurities with NO_x gas on TiO_2 surface for photo-reaction. On the other hand, the sample (d) was also observed to exhibit lower NO_x gas decomposition activity than that of the sample (c). Two reasons are considered for the understanding; one is the decrease of specific surface area (referred to Fig. 6) and the other is the breakage of Ti–C bonding (referred to Fig. 10) due to the high heating temperature (400 °C). Nevertheless, the product (d) heated at 400 °C was still showing a higher activity toward NO_x gas decomposition in visible region compared to the unheated sample (b) due to the existence of C–O bonding (carbonate species), which has been well consistent with other published results [18,19,22].

Particularly with respect to the photo-catalytic ability of Ti–C bonding formed with replacement of O by C, few reports have discussed [21], although such bonding is expected to form similar to that of Ti–N, Ti–S bonding in the N-doped and S-doped TiO_2. One reason may lie at the relative instability of Ti–C bonding. The results shown in Fig. 10 indicated that Ti–C bonding was remaining with the sample prepared at 200 °C heating and disappeared from the sample prepared at 400 °C heating-operation. The results shown in Fig. 7 indicated that both Ti–C and C–O bindings contributed to the photo-catalytic activity. Until now, for carbon doping to TiO_2, lots of high thermal processes have been introduced [18,19,21]. However, few results have obtained both Ti–C and C–O bondings. When TiC is used as starting materials, it is difficult to obtain C–O bonding via oxidization of TiC [21]. When TiO_2 is used as starting materials, heated with other carbon source, normally the relatively thermal stable C–O bonding is obtained [34]. With our research, mechanochemical treatment was operated at room temperature, allowing the formation of both bindings without concern over the problem of instability. These two bindings are stable at even 200 °C heating operation for the removal of surface impurities. This process offers an easy operation to obtain carbon doped TiO_2 with both C–Ti and C–O bindings, which contribute the high activity for NO_x gas decomposition even with irradiation under visible light.

5. Conclusion

Co-grinding of TiO_2 with ethanol, followed by heating enables us to synthesize the carbon doped TiO_2. The most excellent photo-catalytic activity of the C-doped TiO_2 in visible irradiation region has been achieved by grinding for 2 h and heating at 200 °C. The grinding TiO_2 with ethanol causes the formation of Ti–C and C–O bindings in the ground product. The both Ti–C and C–O bindings are maintained by heating at 200 °C. Further heating the product at 400 °C causes the dissociation of Ti–C bindings in the product, whilst the C–O bindings are still maintained in the product. This result induces the decrease in the photo-catalytic activity of the product heated at 400 °C.

Acknowledgement

One of the authors (I.C.K.) is grateful to the Korean Government (MOST) for the financial support provided through the Korea Science and Engineering Foundation Grant (No. 2005-215-D00146).

References

[1] A. Linsebigler, G. Lu, J.T. Yates Jr., Chem. Rev. 95 (1995) 735–758.
[2] M.R. Hoffmann, S.T. Martin, W.Y. Choi, D.W. Bahnemann, Chem. Rev. 95 (1995) 69–96.
[3] N. Serpone, E. Pilezzetti (Eds.), Photocatalysis: Fundamentals and Applications, Wiley/Interscience, New York, 1989.
[4] A. Fujishima, K. Honda, Nature 238 (1972) 37–38.
[5] S.U.M. Khan, J. Akikusa, Int. J. Hydrogen Energy 27 (2002) 863–870.
[6] B. Òregan, M. Grätzel, Nature 353 (1991) 737–740.
[7] K.I. Hadjiivanov, D.K. Klissurski, Chem. Soc. Rev. 25 (1996) 61–69.
[8] A. Heller, Acc. Chem. Res. 28 (1995) 503–508.
[9] I.C. Kang, Q. Zhang, J. Kano, S. Yin, T. Sato, F. Saito, J. Photochem. Photobiol. A: Chem. 189 (2007) 232–238.
[10] R. Asahi, T. Morikawa, T. Ohwaki, K. Aoki, Y. Taga, Science 293 (2001) 269–271.
[11] H. Irie, Y. Watanabe, K. Hashimoto, J. Phys. Chem. B 107 (2003) 5483–5486.
[12] S. Yin, H. Yamaki, Q. Zhang, M. Komatsu, J. Wang, Q. Tang, F. Saito, T. Sato, Solid State Ionics 172 (2004) 205–209.
[13] M. Janus, M. Inagaki, B. Tryba, M. Toyoda, A.W. Morawski, Appl. Catal. B: Environ. 63 (2006) 272–276.
[14] H. Wang, J.P. Lewis, J. Phys. Condens. Mater. 17 (2005) L203–L209.
[15] S.U.M. Khan, M. Al-shahry, W.B. Ingler Jr., Science 297 (2002) 2243–2244.
[16] P. Milani, E. Barborini, A.M. Conti, I. Kholmanov, P. Piseri, A. Podestà, C. Cepek, O. Sakho, R. Macovez, M. Sancrotti, Adv. Mater. 17 (2005) 1842–1846.
[17] C. Xu, Y.A. Shaban, W.B. Ingler Jr., S.U.M. Khan, Solar Energy Mater. Solar Cells 91 (2007) 938–943.
[18] X. Wang, S. Meng, X. Zhang, H. Wang, W. Zhong, Q. Du, Chem. Phys. Lett. 444 (2007) 292–296.
[19] Y. Li, D. Hwang, N. Lee, S. Kim, Chem. Phys. Lett. 404 (2005) 25–29.
[20] W. Ren, Z. Ai, F. Jia, L. Zhang, X. Fan, Z. Zou, Appl. Catal. B: Environ. 69 (2007) 138–144.
[21] H. Irie, Y. Watanabe, K. Hashimoto, Chem. Lett. 32 (2003) 772–773.
[22] H. Kamisaka, T. Adachi, K. Yamashita, J. Chem. Phys. 123 (2005) 084704.
[23] T. Ohno, M. Akiyoshi, T. Umebayashi, K. Asai, T. Mitsui, M. Matsumura, Appl. Catal. A: Gen. 265 (2004) 115–121.
[24] Q. Zhang, J. Wang, S. Yin, T. Sato, F. Saito, J. Am. Ceram. Soc. 87 (2004) 1161–1163.
[25] K. Takeshita, A. Yamakata, T. Ishibashi, H. Onishi, K. Nishijima, T. Ohno, J. Photochem. Photobiol. A: Chem. 177 (2006) 269–275.
[26] S. Klosek, D. Raftery, J. Phys. Chem. B 105 (2001) 2815–2819.
[27] M. Anpo, M. Takeuchi, J. Catal. 216 (2003) 505–516.
[28] H.H. Ou, S.L. Lo, J. Mol. Catal. A: Chem. 275 (2007) 200–205.
[29] T. Ihara, M. Miyoshi, Y. Iriyama, O. Matsumoto, S. Sugihara, Appl. Catal. B 42 (2003) 403–409.
[30] S. Yin, H. Hasegawa, D. Maeda, M. Ishitsuka, T. Sato, J. Photochem. Photobiol. A Chem. 163 (2004) 1–8.
[31] D.C. Hurum, A.G. Agrios, K.A. Gray, T. Rajh, M.C. Thurnauer, J. Phys. Chem. B 107 (2003) 4545–4549.
[32] W.C. Wu, C.C. Chuang, J.L. Lin, J. Phys. Chem. B 104 (2000) 8719–8724.
[33] G.A.M. Hussein, N. Sheppard, M.I. Zaki, R.B. Fahim, J. Chem. Soc., Faraday Trans. 87 (1991) 2661–2668.
[34] C.D. Valentin, G. Pacchioni, A. Selloni, Chem. Mater. 17 (2005) 6656–6665.